Using Graphs to Quantify Energetic and Structural Order in Semicrystalline Oligothiophene Thin Films - Supplementary Information

Ellen Van,[†] Matthew Jones,[‡] Eric Jankowski,[‡] and Olga Wodo[*,¶]

[†]*Department of Mechanical and Aerospace Engineering, University at Buffalo, Buffalo, New York, USA*

[‡]*Micron School of Materials Science and Engineering, Boise State University, Boise, Idaho, USA*

[¶]*Department of Materials Design and Innovation, University at Buffalo, Buffalo, New York, USA*

E-mail: olgawodo@buffalo.edu

Contents

S1 Molecular Dynamics Force Fields and Computation Hardware

There were two MD forcefields used in this investigation, one for generating the initial coarse-grained morphologies, and an atomistic forcefield used for equilibration during the fine-graining process. The dimensionless forcefield parameters and the corresponding base units are listed here.

S1.1 Coarse-Grained Molecular Dynamics

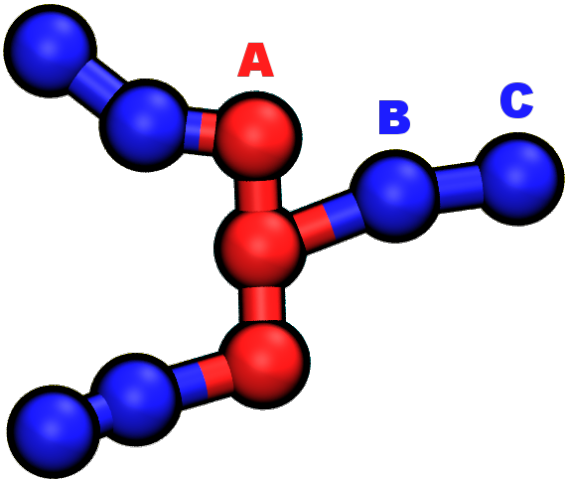

Figure S1.1.1: Molecular structures of a 3-mer of P3HT in the coarse-grained representation. The red beads (denoted 'A') correspond to the thiophene rings that form the chain backbone. The hexyl sidechain is denoted by the blue beads ('B' and 'C')

The coarse-grained forcefield is the same as shown in Jankowski et al 2013,[1] and Marsh et al 2014,[2] which in turn was adapted from the atomistically-derived forcefield of Schwarz et al 2013.[3] The bonded and non-bonded pair potential parameters used in these investigations are shown below.

Table S1.1.1: Non-bonded interaction parameters used in the CGMD simulations. Heterogeneous atom pair interactions $\sigma_{ij} = \sqrt{\sigma_i \sigma_j}$ and $\epsilon_{ij} = \sqrt{\epsilon_i \epsilon_j}$. Pair interactions are defined by a Lennard-Jones potential: $U_{pair}(r) = 4\epsilon \left[\left(\frac{\sigma}{r}\right)^{12} - \left(\frac{\sigma}{r}\right)^{6} \right]$.

Bead Type	σ (Å)	ϵ (kcal mol^{-1})
A	3.000	0.777
B	3.000	0.388
B	3.000	0.388

Table S1.1.2: Bond-stretching parameters used in the MD simulations. Bonds are defined by the following potential: $U_{bond}(r) = k_b(r - r_0)^2$.

Bond Type	r_0 (Å)	k_b (kcal mol^{-1} Å^{-2})
A-A	4.200	2.159
A-B	4.200	2.159
B-C	4.200	2.159

Table S1.1.3: Angle-bending parameters used in the MD simulations. Angles are defined by the following potential: $U_{angle}(\theta) = k_a(\theta - \theta_0)^2$.

Angle Type	θ_0 (rad)	k_a (kcal mol^{-1} rad^{-2})
A-A-A	3.140	2.332
A-A-B	2.130	2.332
A-B-C	3.140	2.332

Table S1.1.4: Torsional parameters used for the single dihedral used in the MD simulations. Torsions are defined by the following potential: $U_{dihedral}(\phi) = k_d(\phi - \phi_0)^2$.

Dihedral Type	ϕ_0 (rad)	k_d (kcal mol^{-1} rad^{-2})
B-A-A-B	3.140	3.886

S1.2 Fine-Grained Atomistic Molecular Dynamics

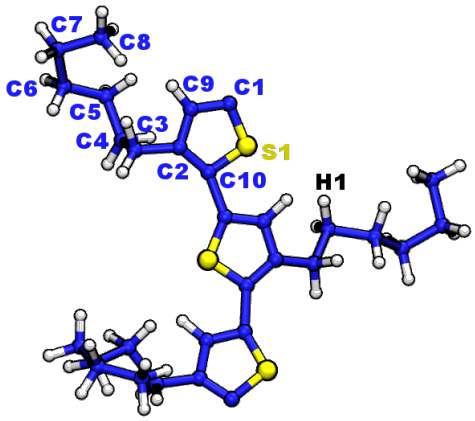

Figure S1.2.1: Molecular structures of the same 3-mer of P3HT as in figure S1.1.1 in the fine-grained (atomistic) representation. Displayed atom types correspond to the forcefield parameters given below. Note that all hydrogens (white atoms) in the molecule are treated equally for simplicity.

The fine-grained forcefield is the same as shown in Bhatta et al. 2013,[4] which was calculated using first-principles molecular structure calculations at the B3LYP/631+(d,p) level, and has been shown to have good experimental agreement with a broad range of structural parameters and materials properties. The bonded and non-bonded pair potential parameters used in these investigations are shown below.

Table S1.2.1: Non-bonded interaction parameters used in the AAMD simulations. Heterogeneous atom pair interactions $\sigma_{ij} = \sqrt{\sigma_i \sigma_j}$ and $\epsilon_{ij} = \sqrt{\epsilon_i \epsilon_j}$. Pair interactions are defined by a Lennard-Jones potential: $U_{pair}(r) = 4\epsilon \left[\left(\frac{\sigma}{r}\right)^{12} - \left(\frac{\sigma}{r}\right)^{6} \right]$.

Bead Type	σ (Å)	ϵ (kcal mol^{-1})
CA1	3.550	0.070
CA2	3.550	0.070
CT	3.500	0.066
H	2.500	0.030
S	3.550	0.250

Table S1.2.2: Bond-stretching parameters used in the MD simulations. Bonds are defined by the following potential: $U_{bond}(r) = k_b(r - r_0)^2$.

Bond Type	r_0 (Å)	k_b (kcal mol^{-1} Å^{-2})
CA1-S	1.734	291.250
CA1-CA2	1.374	514.270
CA2-CA2	1.433	453.100
CA2-CT	1.509	288.820
CT-CT	1.542	268.000
CT-H	1.098	327.545
CA2-H	1.082	370.630
CA1-CA1	1.450	392.290

Table S1.2.3: Angle-bending parameters used in the MD simulations. Angles are defined by the following potential: $U_{angle}(\theta) = k_a(\theta - \theta_0)^2$.

Angle Type	θ_0 (rad)	k_a (kcal mol^{-1} rad^{-2})
CA1-S-CA1	1.619	86.360
S-CA1-CA2	1.925	86.360
CA1-CA2-CA2	1.978	39.582
CA2-CA2-H	2.159	35.263
CA1-CA1-CA2	2.271	54.694
CA1-CA2-H	2.146	35.263
S-CA1-CA1	2.087	41.740
CA2-CA2-CT	2.153	166.545
CA1-CA2-CT	2.174	166.320
CA2-CT-H	1.906	74.060
CT-CT-CT	1.967	58.350
CT-CT-H	1.932	37.500
H-CT-H	1.881	33.000

Table S1.2.4: Torsional parameters used for the single dihedral used in the MD simulations. Torsions are defined by the following potential: $U_{dihedral}(\phi) = \sum_{n=0}^{4} k_{d,n} \cos^n(\phi)$.

Dihedral Type	$k_{d,0}$ (kcal mol^{-1})	$k_{d,1}$ (kcal mol^{-1})	$k_{d,2}$ (kcal mol^{-1})	$k_{d,3}$ (kcal mol^{-1})	$k_{d,4}$ (kcal mol^{-1})
S-CA1-CA1-S	2.953	0.157	-4.233	0.398	1.886
CA2-CA2-CT-CT	0.318	1.127	14.143	-22.297	6.719
CA2-CA1-S-CA1	126.320	-109.81	-19.738	-25.303	28.530
CA1-CA2-CA2-CA1	126.320	-109.81	-19.738	-25.303	28.530
CA2-CA2-CA1-S	126.320	-109.81	-19.738	-25.303	28.530
CA2-CT-CT-CT	2.447	-6.395	10.747	30.695	11.139
CT-CT-CT-CT	1.940	-3.683	1.339	7.730	0.7671
S-CA1-CA1-CA2	2.953	-0.157	-4.233	-0.398	1.886
CT-CA2-CA2-CA1	117.650	238.260	205.960	112.810	27.467
CA2-CA2-CA1-CA1	75.595	116.000	42.679	-1.528	-3.814
CA1-CA1-S-CA1	158.700	418.340	521.330	376.730	115.120

S1.3 Computational Hardware

- The coarse-grained molecular dynamics simulations to obtain the relaxed structures were performed on the Janus supercomputer at the University of Colorado Boulder, using a combination of NVIDIA c2050 (driven by a 2.67 GHz Intel Nehalem CPU) and c2090 GPUs (driven by a 2.8 GHz Intel Westmere CPU).

- The fine-graining process and subsequent molecular dynamics simulations were performed using the Kestrel supercomputer at Boise State University, using NVIDIA K20 GPUs driven by 2.6 GHz Intel Sandy Bridge CPUs.

- The quantum chemical calculations and kinetic Monte Carlo mobility calculations were performed using both Kestrel and the Fry supercomputer, also at Boise State using 2.1 GHz Intel Broadwell CPUs.

S2 Determining Equilibration

The simulated systems were considered equilibrated if it had run for sufficiently long that there were at least 20 statistically independent snapshots at the end of a trajectory. Statistical independence was defined according to the autocorrelation time of the potential energy of the system, which is used here as a proxy for structural evolution. The autocorrelation time, a was calculated as the temporal location of the first zero of:

$$C(dt) = \frac{\langle (\mathrm{PE}(t) - A)(\mathrm{PE}(t + dt) - A) \rangle}{\varsigma^2}, \tag{1}$$

where $\mathrm{PE}(t)$ is the instantaneous potential energy at time, t, with average value, A, and variance ς, over potential energy subsets of the time series. This criterion is therefore satisfied if there exists a subset with range $t_{\max} - t_{\min} > 20a$.

S3 Fine-graining Molecular Dynamics

The fine-graining process involves the sequential execution of molecular dynamics simulations to gradually remove unphysical conformations of atoms from the system, in order to generate a realistic final atomistic morphology. As many atom pairs in the system have significant overlap at distances $r << \sigma$, initially many of the inter-atomic forces are high enough that atoms can move many periodic boxes in a single timestep, creating numerical instabilities and breaking the simulation. This necessitates the use of 'soft' inter-atomic potentials (such as Dissipative Particle Dynamics (DPD) instead of conventional Lennard-Jones (LJ)), and extremely small timesteps that are increased gradually as the simulation chain progresses.

In the current investigation, the fine-graining utilized a chain of 8 simulations, the important characteristics of which are described in table S3.0.1. For each simulation phase, trajectory snapshots were taken 100 times and energies logged 1000 times periodically, regardless of total duration.

Table S3.0.1: Molecular dynamics simulation parameters for each phase of the fine-graining process.
† The goal of phase one is to relax the intra-molecular constraints of the molecules, and so the simulation was terminated as soon as the kinetic energy reached a minimum (defined as the trajectory snapshot after which the kinetic energy increase monotonically for 5 subsequent snapshots). Generally, this occurred within the first thousand timesteps.
‡ Preliminary work has shown that equilibrating the final phase for 1×10^8 timesteps does not significantly alter the final, equilibrated structure so the value of 1×10^5 was selected in the interest of computational efficiency.

Phase ID	Pair Type	Timestep, τ (s)	Duration (τ)
1	None	3.5×10^{-16}	$1 \times 10^{5,\dagger}$
2	DPD	3.5×10^{-16}	1×10^4
3	LJ	3.5×10^{-23}	1×10^3
4	LJ	3.5×10^{-22}	1×10^3
5	LJ	3.5×10^{-21}	1×10^3
6	LJ	3.5×10^{-20}	1×10^4
7	LJ	3.5×10^{-19}	1×10^5
8	LJ	3.5×10^{-18}	$1 \times 10^{5,\ddagger}$

S4 Effect of sample rotation on selected descriptors

Morphologies generated for this study assumed periodic boundary conditions on all boundaries of the cube. When morphologies were represented as a graph, one of the boundaries was arbitrarily cut. We selected the boundary connecting top and bottom faces of the sample, cut all edges intersecting with this boundary and subsequently connected the tangling edges with the meta vertex representing the electrodes. Since the choice of the boundary to be cut was arbitrary, we perform the analysis to check the effect of sample rotation. Table S4.0.1 includes the descriptors for five morphologies with three rotational configurations. These descriptors demonstrate that trends reported in the main text are insensitive to the sample rotation.

Table S4.0.1: First order descriptors for five morphologies and three rotations. Symbols used as in Table 1 in the main text.

	$tortuosity$	$\mathcal{E}_{intra}$	$\mathcal{E}_{inter}$	f_{CC}^{useful}	$\mathcal{N}_{BB}$	$\mathcal{N}_{SCh}$
$T = 1.5$ rot 0	1.10	10,889	3,340	1	1	1
rot 1	1.34	10,971	3,334	1	4	1
rot 2	1.70	11,045	3,373	1	3	1
$T = 1.75$ rot 0	1.28	6,931	3,393	1	3	1
rot 1	1.30	6,887	3,392	1	4	1
rot 2	1.26	6,921	3,381	1	2	1
$T = 2.0$ rot 0	1.29	6,005	3,403	1	1	1
rot 1	1.28	6,031	3,392	1	2	1
rot 2	1.31	6,038	3,417	1	2	1
$T = 2.25$ rot 0	1.31	5,497	3,423	1	1	1
rot 1	1.30	5,537	3,421	1	1	1
rot 2	1.28	5,489	3,423	1	1	1
$T = 2.5$ rot 0	1.33	5,050	3,437	1	3	1
rot 1	1.32	5,005	3,420	1	1	1
rot 2	1.31	5,010	3,425	1	4	1

S5 Correlation studies between morphological descriptors

Figure S5.0.1 depicts the correlations between the shortest and fastest pathways in thermal annealing dataset. Each panel on this figure depicts 3750 points corresponding to pathways from each backbone vertex in the graph to the meta vertex representing electrode. Each point is characterized by length of the shortest pathway and travel time along the fastest pathway. Results confirm our observation made in the main document regarding well-ordered morphologies (e.g. $T = 1.5$) that the shortest pathways are also the fastest pathways.

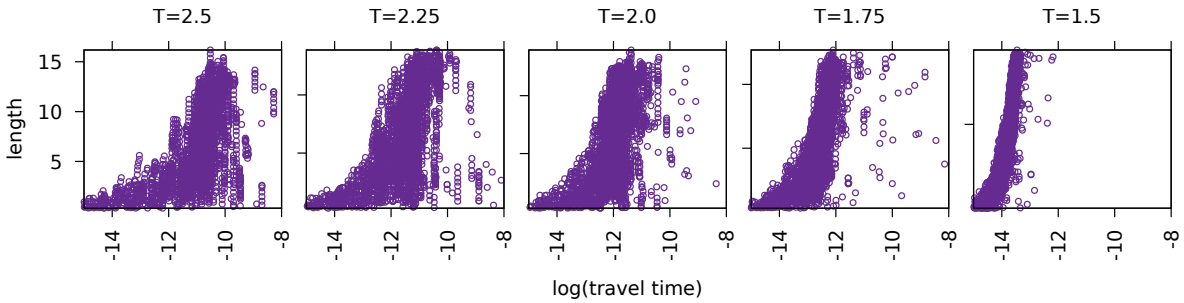

Figure S5.0.1: Correlation between the length of the shortest pathway and the travel time along the fastest pathways for increasing annealing time from $T = 1.5$ to $T = 2.5$.

References

(1) Jankowski, E.; Marsh, H. S.; Jayaraman, A. *Macromolecules* **2013**, *46*, 5775–5785.

(2) Marsh, H. S.; Jankowski, E.; Jayaraman, A. *Macromolecules* **2014**, *47*, 2736–2747.

(3) Schwarz, K. N.; Kee, T. W.; Huang, D. M. *Nanoscale* **2013**, *5*, 2017–2027.

(4) Bhatta, R. S.; Yimer, Y. Y.; Perry, D. S.; Tsige, M. *The Journal of Physical Chemistry B* **2013**, *117*, 10035–10045.